ADVANCED ENERGY MATERIALS
www.advenergymat.de

Countersolvent Electrolytes for Lithium-Metal Batteries

Nan Piao, Xiao Ji, Hong Xu, Xiulin Fan, Long Chen, Sufu Liu, Mounesha N. Garaga, Steven G. Greenbaum, Li Wang, Chunsheng Wang,* and Xiangming He**

Development of electrolytes that simultaneously have high ionic conductivity, wide electrochemical window, and lithium dendrite suppression ability is urgently required for high-energy lithium-metal batteries (LMBs). Herein, an electrolyte is designed by adding a countersolvent into LiFSI/DMC (lithium bis(fluorosulfonyl)amide/dimethyl carbonate) electrolytes, forming countersolvent electrolytes, in which the countersolvent is immiscible with the salt but miscible with the carbonate solvents. The solvation structure and unique properties of the countersolvent electrolyte are investigated by combining electroanalytical technology with a Molecular Dynamics simulation. Introducing the countersolvent alters the coordination shell of Li^+ cations and enhances the interaction between Li^+ cations and FSI^- anions, which leads to the formation of a LiF-rich solid electrolyte interphase, arising from the preferential reduction of FSI^- anions. Notably, the countersolvent electrolyte suppresses Li dendrites and enables stable cycling performance of a Li||NCM622 battery at a high cut-off voltage of 4.6 V at both 25 and 60 °C. This study provides an avenue to understand and design electrolytes for high-energy LMBs in the future.

1. Introduction

The rapid development of electric vehicles and stationary energy storage systems requests high-energy batteries, which cannot be met by conventional lithium-ion batteries (LIBs) that are approaching to their theoretical specific energy density.[1,2] With an ultrahigh theoretical specific capacity (3860 mAh g^{-1}) and the lowest electrochemical potential [−3.04 V versus standard hydrogen electrode (SHE)], lithium-metal anode is considered to be a promising anode for the next-generation high-energy batteries.[1] However, Li dendrites growth in lithium-metal batteries (LMBs) reduces Coulombic efficiency (CE) of Li plating and stripping and causes safety concern.[3,4] The commercial electrolyte with the $LiPF_6$ salt and carbonate solvents for the graphite anode is not suitable for the lithium-metal anode.[5] Introducing lithium host,[6,7] artificial protective interface,[8,9] and regulating electrolytes (lithium salts, solvents, or additives)[10–14] have been demonstrated as effective approaches to suppress Li dendrites.

In recent years, "Super-concentrated electrolyte"[15] ["Solvent-in-salt"[16] or "Highly concentrated electrolyte (HCE)"][5] shows a high capability to suppress Li dendrites and stabilize high-voltage cathodes, because the high concentration of FSI^- anions facilitates the formation of a high F-rich interphase on both Li metal and cathode surfaces.[17] However, high viscosity and high cost restrict its practical application.[18] To address the above issues, the inert diluent solvent has been introduced to the HCE, forming "Localized high-concentration electrolyte",[12,19–21] or "Pseudo-concentrated electrolyte"[22,23] with the low viscosity, high wettability, and high Li-ion conductivity. Herein, we report that the local-concentrated electrolyte is in an intermediate state before lithium salt precipitation and the inert diluent solvent is a countersolvent, which not only contributes to the formation of local 3D regions, but also saturates the electrolyte at a low salt concentration by the countersolvent effect and promotes the association of Li^+ and FSI^-, which have not been fully explored yet.

In order to meet the battery requirement on high temperature (60 °C), we introduce the 1,1,2,2-Tetrafluoroethyl-2,2,3,3-tetrafluoropropylether (TTE) with a high boiling point ($T_{b.p.}$ = 92 °C) as the countersolvent into the LiFSI/DMC (lithium bis(fluorosulfonyl)amide/dimethyl carbonate) electrolyte (DMC:TTE, 1:1 by mol) forming a countersolvent electrolyte and systemically investigate the solvation structure of this electrolyte. Both experimental and computational studies demonstrate that adding countersolvent into electrolytes could significantly reduce the solvation degree of Li^+ ions but increase the binding strength of Li^+ ions with anions, which is favor for forming an inorganic LiF-rich solid electrolyte interphase (SEI) on Li metal. The countersolvent in the electrolyte could also separately manipulate physical property (viscosity, ionic conductivity, etc.) and chemical/electrochemical property (electrochemical stability window, etc.). The countersolvent electrolyte not

N. Piao, Prof. H. Xu, Prof. L. Wang, Prof. X. M. He
Institute of Nuclear and New Energy Technology
Tsinghua University
Beijing 100084, China
E-mail: wang-l@mail.tsinghua.edu.cn; hexm@tsinghua.edu.cn
Dr. X. Ji, Dr. X. L. Fan, Dr. L. Chen, S. F. Liu, Prof. C. S. Wang
Department of Chemical and Biomolecular Engineering
University of Maryland
College Park, MD 20742, USA
E-mail: cswang@umd.edu
Dr. M. N. Garaga, Prof. S. G. Greenbaum
Department of Physics and Astronomy
Hunter College
City University of New York
New York, NY 10065, USA
The ORCID identification number(s) for the author(s) of this article can be found under https://doi.org/10.1002/aenm.201903568.

DOI: 10.1002/aenm.201903568

only forms an Li dendrites-free SEI on Li metal, enabling a high Li plating/stripping CE and a long-term cycling performance for Li-metal anode, but also has a good compatibility with NMC622 cathode under a high voltage, thus exhibiting a stable cycling performances of Li‖NCM622 battery at a high cut-off voltage of 4.6 V at both 25 and 60 °C. The understanding of the countersolvent electrolyte will provide a guideline for designing the next-generation electrolytes for high-energy batteries.

2. Results and Discussion

2.1. Physicochemical Properties

Highly fluorinated diluent solvents normally have a high thermal stability, high oxidation resistance, and high non-flammability, which will well meet the requirements of high-energy batteries.[24,25] TTE as a kind of hydrofluoroether with a high boiling point (92 °C) was selected as the countersolvent in this study. The physical properties of the LiFSI/DMC electrolytes with different salt and countersolvent concentrations are shown in **Figure 1** and Table S1 in the Supporting Information. As shown in Figure 1, for the LiFSI/DMC electrolyte, viscosity of the electrolyte monotonously increases as the molar ratio of the lithium salt increases. When the molar ratio of LiFSI to DMC increases from 1:12 (D1) to 1:1.5 (D7), corresponding to the electrolyte concentration increasing from 0.91 to 4.65 mol dm^{-3}, the viscosity of the electrolyte exponentially increases from 1.49 to 94.26 mPa s. However, the conductivity first increases from 8 to 12 mS cm^{-1} as the molar ratio of LiFSI/DMC increases from 1:12 (D1) to 1:6 (D3), and then decreases to 2.50 mS cm^{-1} when the LiFSI/DMC ratio reaches 1:1.5 (D7). For the LiFSI/DMC/TTE countersolvent electrolyte, adding TTE countersolvent into LiFSI/DMC electrolytes can reduce the concentration and viscosity while maintain the ionic conductivity. When the molar ratio of LiFSI/DMC/TTE increases to 1:1.5:1.5 (T3), the viscosity (9.95 mPa s) reduces to only 1/10 of D7, while the conductivity still maintains a similar value of 1.70 mS cm^{-1}. As shown in the inset picture in Figure 1, all the electrolytes on the left-hand side of T3 (includes T3) are transparent liquid. However, further adding TTE to 1:1:2 (T4) leads to the crystallization in the solution due to the countersolvent effect of TTE. Upon further increasing the TTE in LiFSI/DMC/TTE to the molar ratio of 1:1.5:2.5, LiFSI salts will immediately precipitate from the electrolyte and the solution turns from transparent to muddy (Figure 1). Based on the physical results, T3 electrolyte (2.27 mol L^{-1}) was selected as a representative countersolvent electrolyte because it is near saturated while still in a stable liquid state. For comparison, D1 electrolyte (0.91 mol L^{-1}), D4 electrolyte (2.41 mol L^{-1}), and D7 electrolyte (4.65 mol L^{-1}) were also investigated.

2.2. Solvation Structure

The structural changes of LiFSI/DMC/TTE electrolytes at different compositions were characterized using Raman spectroscopy. As shown in **Figure 2**a, as the LiFSI concentration increases (from D1 to D7) in the LiFSI/DMC electrolyte, the peak of the free DMC molecule at about 913 cm^{-1} (O—CH_3 stretching vibration)[26] gradually weakens and eventually disappears at high LiFSI concentrations (D6 and D7). Li^+-solvated DMC peaks (at 931 and 871 cm^{-1}) emerge and increase from D1 to D7 because more DMC molecules are solvated with Li^+ ions as the LiFSI concentration increases.[15] Besides, the increase in the LiFSI concentration also causes the peak shift from 727 to 747 cm^{-1}, since the association of Li^+ ions with FSI^- anions is also increased. For the LiFSI/DMC/TTE electrolyte (T3) (Figure 2b), the peak assigned to Li^+-coordinated FSI^- (near 750 cm^{-1}) shifts to the left, which means that introducing of TTE countersolvent enhances the coordination strength between Li^+ cations and FSI^- anions.

Molecular Dynamics (MD) simulation was performed to further investigate the solvation structure of electrolytes. Figure 2c–f shows snapshots of simulated D1, D4, D7, and T3 electrolytes. The solvents in the first coordinated shell are depicted by ball and stick model, while the wireframes represent the free solvent. As the salt concentration increases from D1, D4, to D7 electrolytes, the proportion of free DMC molecules in the electrolyte is greatly reduced, and only a small amount of free DMC molecules (blue wireframes) are present in D7. It

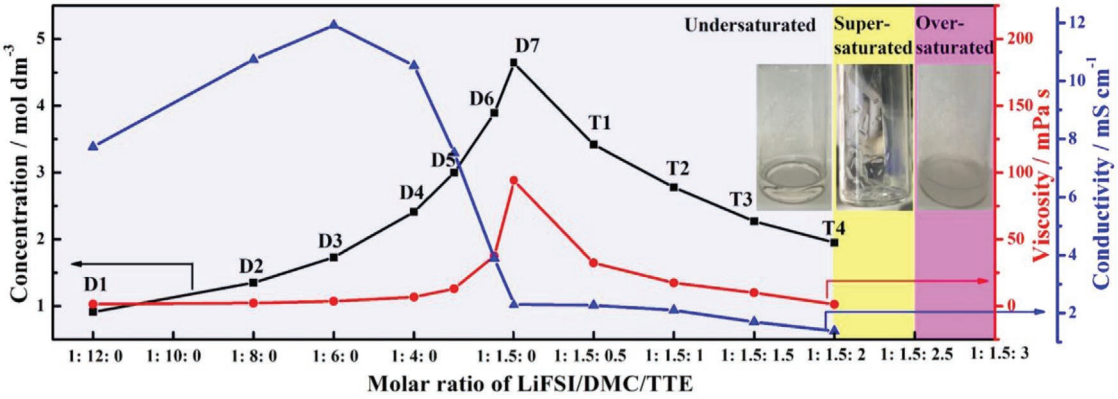

Figure 1. Concentration, viscosity, and conductivity of LiFSI/DMC/TTE electrolytes at different compositions. The electrolytes show three states: 1) undersaturated electrolytes (blue region); the electrolytes in this region are transparent liquid. 2) Supersaturated electrolytes (yellow region); needle-like crystals precipitate from the electrolyte after standing for about two weeks. 3) Oversaturated electrolytes (pink region); and the salt precipitates immediately after adding TTE.

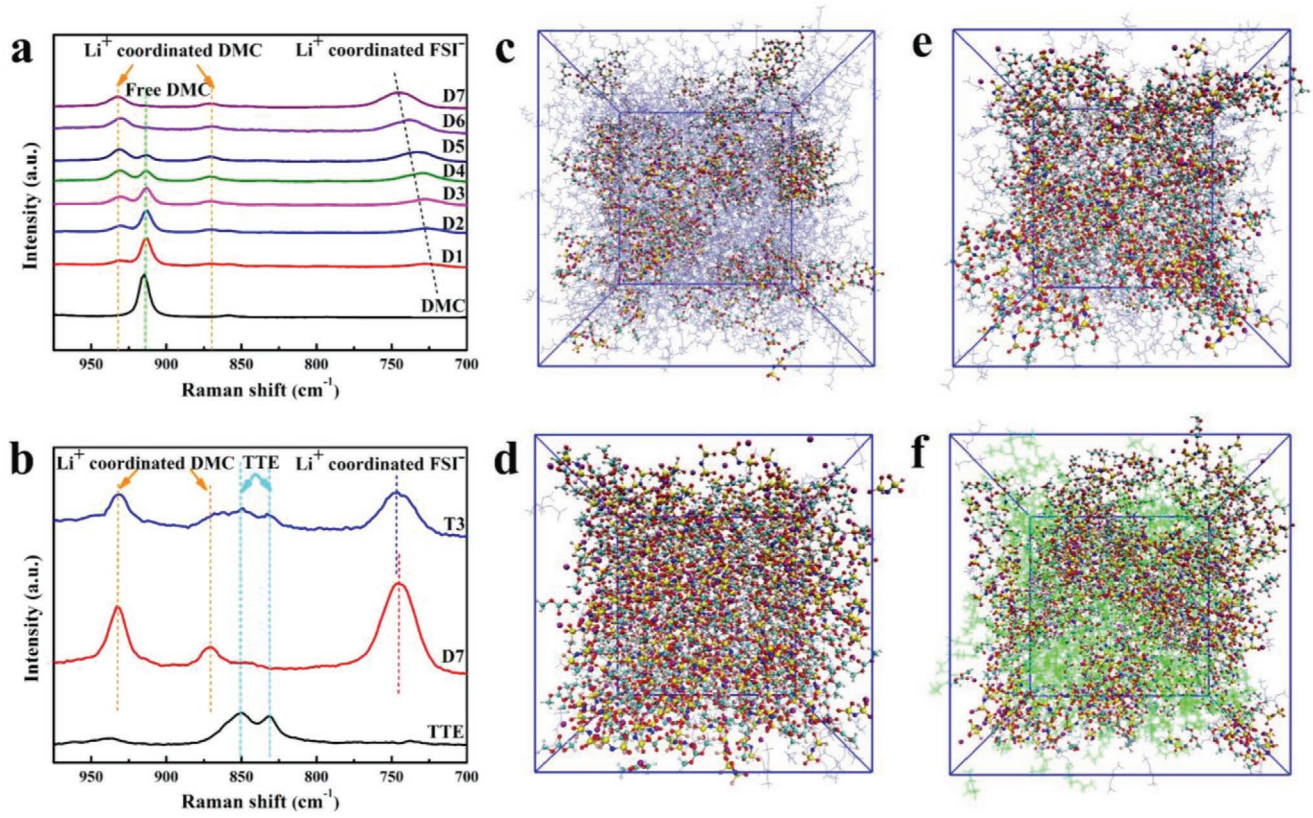

Figure 2. Raman spectra of a) DMC and LiFSI/DMC electrolytes at different compositions (D1–D7) and b) TTE, D7, and T3 in the range of 700–975 cm^{-1}. Snapshots of different LiFSI/DMC electrolytes obtained by MD simulation at 298 K: c) D1, d) D4, e) D7, and f) T3. The Li^+ ions and their first coordinated shells (within 2.75 Å of Li^+ ions) are presented by ball and stick model, while the wireframes stand for free DMC (blue) and free TTE (green), respectively.

can be observed that Li^+-DMC and Li^+-FSI^- are the main interactions in D7, forming a 3D network. The local 3D structure of the T3 electrolyte is similar to D7 but is divided by TTE into separate regions. According to the radial distribution function and coordination numbers of D1, D4, D7, and T3 (Figure S1, Supporting Information), the O* (O atom from FSI^- anion) and O = (O atom connected to one C atom in DMC molecule) are mainly account for the first Li^+ coordinated shell (2.75 Å within Li^+ cations). And the N* (N atom from FSI^- anion) and —O— (O atom from TTE molecule) are mainly exist at about 4 Å from Li^+ cations, which means they are not directly solvate with Li^+ cations. Structures of LiFSI, DMC, and TTE molecules and the atom charges for the MD simulations are shown in Figure S2 in the Supporting Information. The detailed MD results are listed in Tables S2 and S3 in the Supporting Information.

According to the statistics of MD simulation, contact ion pairs (CIPs, FSI^- coordinating 1 Li^+) and aggregate clusters (AGGs, FSI^- coordinating to 2 or more Li^+) are dominant in D1, D4, D7, and T3 electrolytes (Figure S3, Supporting Information). An increase in salt concentration results in a decrease in the proportion of CIPs and enhanced ion association from AGGs-(I) (FSI^- coordinating to 2 Li^+) to AGGs-(II) (FSI^- coordinating to 3 Li^+). Furthermore, the percentage of AGGs-(III) (FSI^- coordinating to 4 and 5 Li^+) is even higher in T3 than that in D7. The solvation state of Li^+ ion in different electrolytes was compared in **Figure 3**. The results indicate that as the salt concentration increases, the proportion of highly FSI^- coordinated Li^+ cation (Li coordinated to three or more FSI^- anions) increases (Figure 3a), and the proportion of highly DMC molecules coordinated Li^+ cation (Li coordinated to three or more DMC molecules) decreases (Figure 3b). Specifically, in D1 and D4 electrolytes, the Li^+ mainly coordinate 2 FSI^-, while in D7 electrolyte, the Li^+ coordinate 3 FSI^-. Meanwhile, Li^+-3 DMC, Li^+-2 DMC, and Li^+-DMC structures dominate D1, D4, and D7 electrolytes, respectively (Figure 3c–e). This is consistent with conventional understanding of solvation structure and is also mutually validated by Raman characterization. A further comparison of the solvated structure of D7 and T3 shows that they generally have a similar structure, which is mainly Li^+-DMC and Li^+-3 FSI^- interactions (Figure 3e,f). However, the amount of Li^+-4 FSI^- or Li^+-5 FSI^- and Li^+-0 DMC coordination significantly increases in T3 electrolyte, because the addition of countersolvent will enhance the association between Li^+ cations and FSI^- anions, causing the electrolyte saturated. Therefore, based on the experiment and calculation, we can obtain a near-saturated electrolyte using the countersolvent at a relatively low salt concentration.

2.3. Li-Metal Plating/Stripping Cycling CE and Stability

The MD simulation demonstrates that the introduced TTE alters the Li^+ coordination shell structure, which will affect

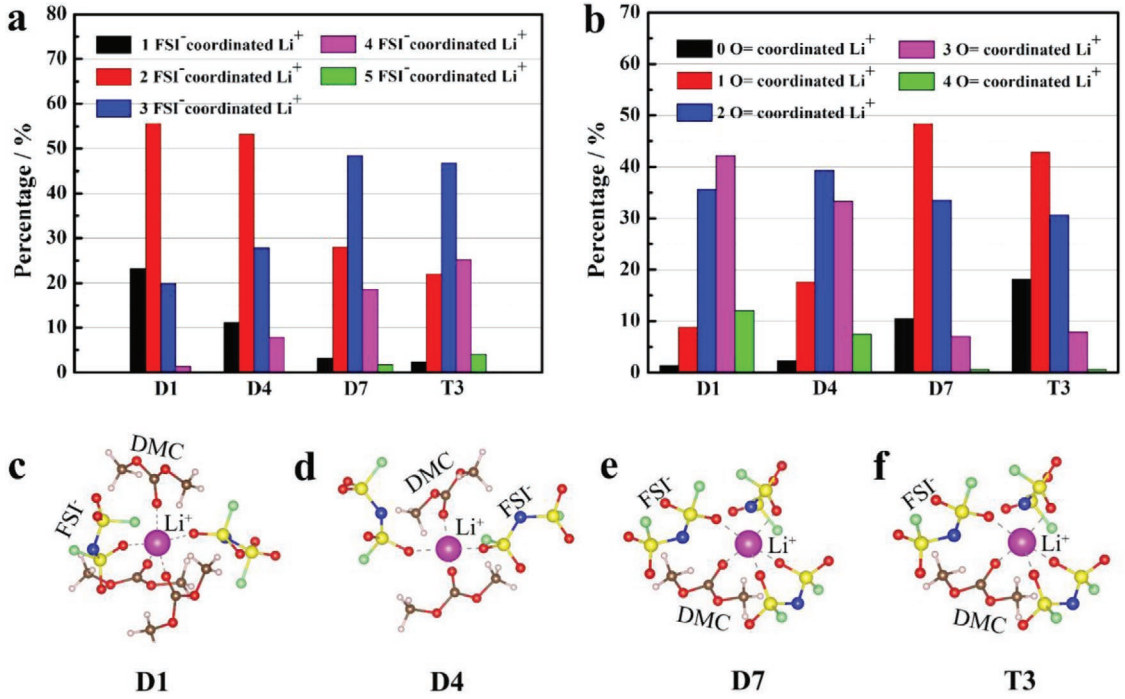

Figure 3. Percentage of Li^+ coordination structure in different electrolytes based on MD simulation. a) Percentage of Li^+ cations, which coordinate with different number of FSI^- anions in D1, D4, D7, and T3. b) Percentage of Li^+ cations, which coordinate with different number of DMC molecules in D1, D4, D7, and T3. (O = stands for O atoms connected to one C atom in DMC). Major Li^+ coordination structure in c) D1, d) D4, e) D7, and f) T3. Balls with various colors represent different atoms; color code: red, O; blue, N; yellow, S; cyan, F; magenta, Li.

the formation of SEI and the cycling stability of Li metal. The CE profiles of Li plating/stripping on Cu measured at a high current density of 1 mA cm^{-2} and a capacity of 1 mAh cm^{-2} in LiFSI/DMC electrolytes at different compositions without TTE countersolvent are shown in **Figure 4**a. The CE increases with the salt concentration in LiFSI/DMC electrolytes. Specifically, at a low salt concentration (D1–D4), the CE is still very low (less than 50%). When the salt concentration increases to D6, the CE increases to 97% in 15 cycles, but it drops quickly after that. When the molar ratio of LiFSI to DMC reaches to 1:1.5 (D7), the CE further increases to above 98% in 50 cycles. Figure 4b compares the Li plating/stripping CE in Li||Cu cells during long-term cycling in D7, T3, and the conventional 1 M $LiPF_6$/EC+DMC (1:1, vol.) electrolytes. The CE in 1 M $LiPF_6$/EC+DMC fluctuates greatly between 80%–95% and then drops after 70 cycles with an initial CE less than 90%. The average CE in D7 electrolyte is 98.3% in initial 200 cycles, but it begins to decay after 200 cycles. Notably, Li plating/stripping in T3 electrolyte achieves a high average CE of 98.6% in 400 cycles at a high current density of 1 mA cm^{-2} and a capacity of 1 mAh cm^{-2}. It is worth noting that a high CE of 99% was achieved in T3 electrolyte at a current density of 0.2 mA cm^{-2} and a capacity of 1 mAh cm^{-2} (Figure S4, Supporting Information). A large overpotential and a high impedance were observed for Li plating on Cu in 1 M $LiPF_6$/EC+DMC, while Li plating in T3 and D7 electrolytes show small overpotentials and low impedances (Figure S5, Supporting Information). Specifically, the resistance of the Li||Cu cell with 1 M $LiPF_6$/EC+DMC is 72.5 Ω, which is much higher than that of D7 (23.8 Ω) and T3 (21.6 Ω). It is believed that the robust SEI with low resistance in T3 electrolytes is responsible for the high CE of Li plating/stripping.[17,19]

The morphology of Li deposition in different electrolytes was observed by scanning electron microscopy (SEM) images (Figure 4c–e). A large amount of lithium dendrites can be observed for lithium deposited in the commercial electrolyte (Figure 4c), and the lithium dendrites expose a large active surface to the electrolyte, which cause side reactions between the lithium metal and the electrolyte, resulting in a low CE. For comparison, the morphology images of lithium deposition in D7 and T3 electrolytes show large Li particles with several micrometers in size. Moreover, the lithium metal particles formed in T3 electrolyte are larger than that in D7 electrolyte, leading a small contact area of Li in T3, which is more conducive to reducing side reactions and improving CE. The photos in the upper right corner of Figure 4c–e show the surface of Li deposited on Cu foils at 1 mA cm^{-2} and 1 mAh cm^{-2}. Due to side reactions, the surface of Li deposited in 1 M $LiPF_6$/EC+DMC is black and uneven, while the surfaces of Li deposited in D7 and T3 electrolytes exhibit a metallic luster. Moreover, the surface of Li deposition in T3 electrolyte is smoother than that in D7, which indicates that the SEI formed in T3 is compact and can effectively prevent the side reactions between Li and the electrolyte.

X-ray photoelectron spectroscopy (XPS) analysis was performed to further study the SEI composition of the deposited Li in different electrolytes (Figure 4f–h). The SEI of the plated Li on Cu foils after 10 cycles at 1 mA cm^{-2} and 1 mAh cm^{-2} were characterized. The results of F 1s spectra show that SEI formed in T3 electrolyte has a stronger LiF peak (684.8 eV) but a weaker

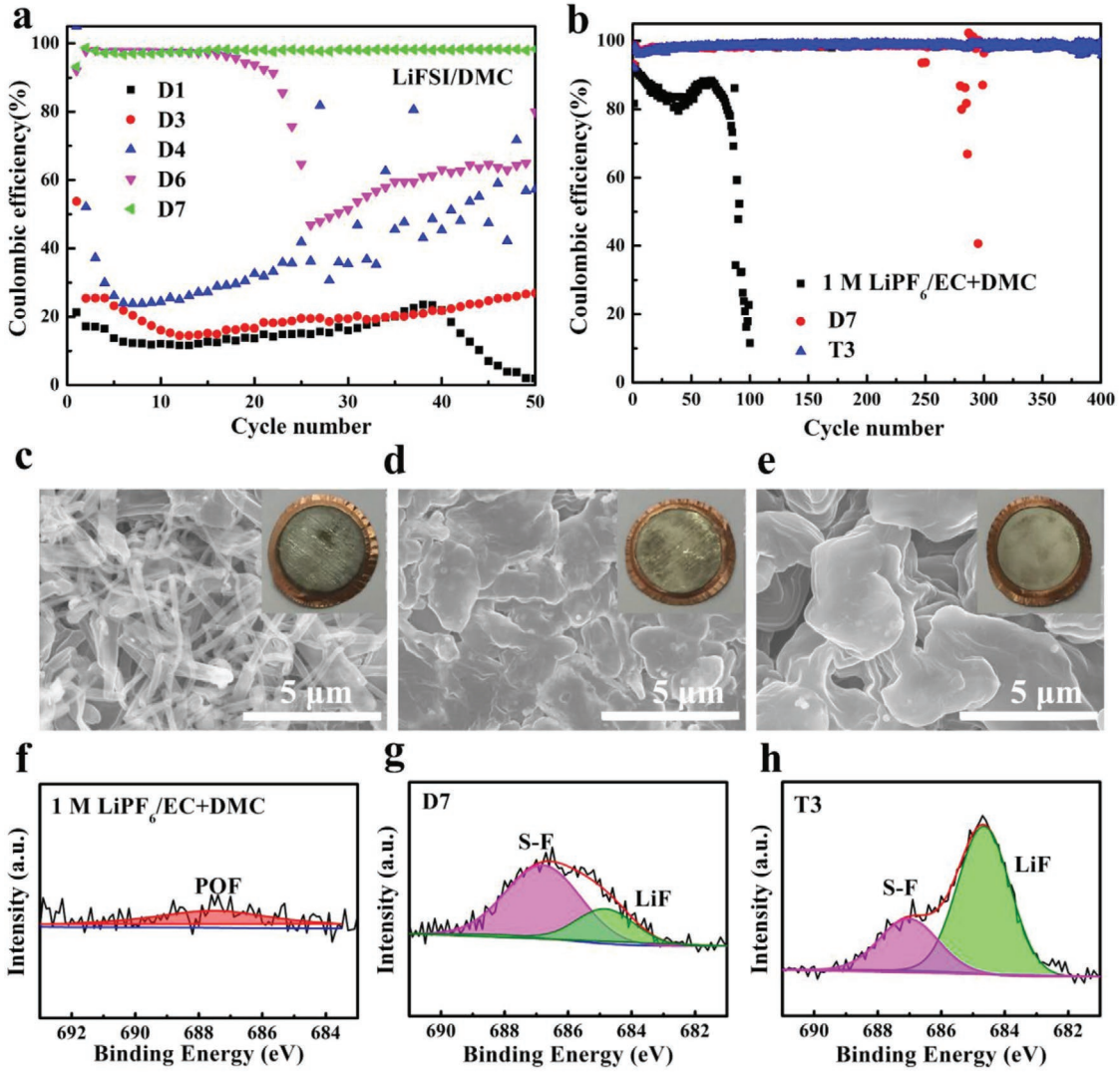

Figure 4. a) CE of Li plating/stripping profiles in LiFSI/DMC electrolytes at different compositions. b) Long-term Li plating/stripping stability in 1 M $LiPF_6$/EC+DMC, D7, and T3 electrolytes. Morphologies of Li plated on Cu foils in c) 1 M $LiPF_6$/EC+DMC, d) D7, and e) T3. F 1s spectra of SEI after the 10 cycles in Li‖Cu cells with f) 1 M $LiPF_6$/EC+DMC, g) D7, and h) T3 electrolytes, respectively. The current density is 1 mA cm^{-2} and the capacity is 1 mAh cm^{-2}.

S—F peak, compared to the SEI formed in D7. As shown in Figure S6 in the Supporting Information, the lowest unoccupied molecular orbital (LUMO) of LiFSI (–0.39 eV) is much lower than that of TTE (1.19 eV), which indicates that LiFSI is much easier to reduce than TTE, so LiF is the main reduction product of LiFSI in T3. The higher LiF content in T3 detected by XPS indicates that LiFSI is more easily decomposed in T3 than D7 due to the higher association of FSI^- anions with Li^+ in T3 electrolyte. The solvated FSI^- anions will enter the inner Helmholtz layer and further decompose when the electrode is polarized, so that more FSI^- anions are reduced on the Li surface to form an LiF-rich SEI.[27] The high content of LiF in the SEI is recognized to be effective to suppress the growth of Li dendrites because its high interfacial energy, which can accelerate surface diffusion and accommodate the large volume change of Li metal. In addition, the high electronic resistance of LiF can prevent electrons from leaking through the SEI and exhibit a superior stability with Li metal. Therefore, the continuous reaction of the electrolyte with Li is restrained, sufficiently decreasing the thickness of Li metal, thus reducing the total Li-ion conduction resistance of the interface,[17,28,29] which was also proved by the reduced interfacial resistance in T3 compared with D7 (Figure S5, Supporting Information). In contrast, for the 1 M $LiPF_6$/EC+DMC electrolyte, only POF peak at 687.5 eV was detected in F 1s spectra because large amount of solvents were reduced along with $LiPF_6$, forming a non-uniform composite SEI.

Li‖Li symmetrical cells were used to compare the long-term cycling stability of Li anode in T3 and 1 M $LiPF_6$/EC+DMC electrolytes. T3 electrolyte enables a 1000 h stable cycling at 1 mA cm^{-2} and 1 mAh cm^{-2} with a voltage hysteresis of ≈38 mV (Figure S7a, Supporting Information). The electrochemical impedance spectroscopy (EIS) of Li‖Li cells in T3 electrolyte before and after 100 h cycling both show much lower resistances than those in the commercial electrolyte (Figure S7b,c,

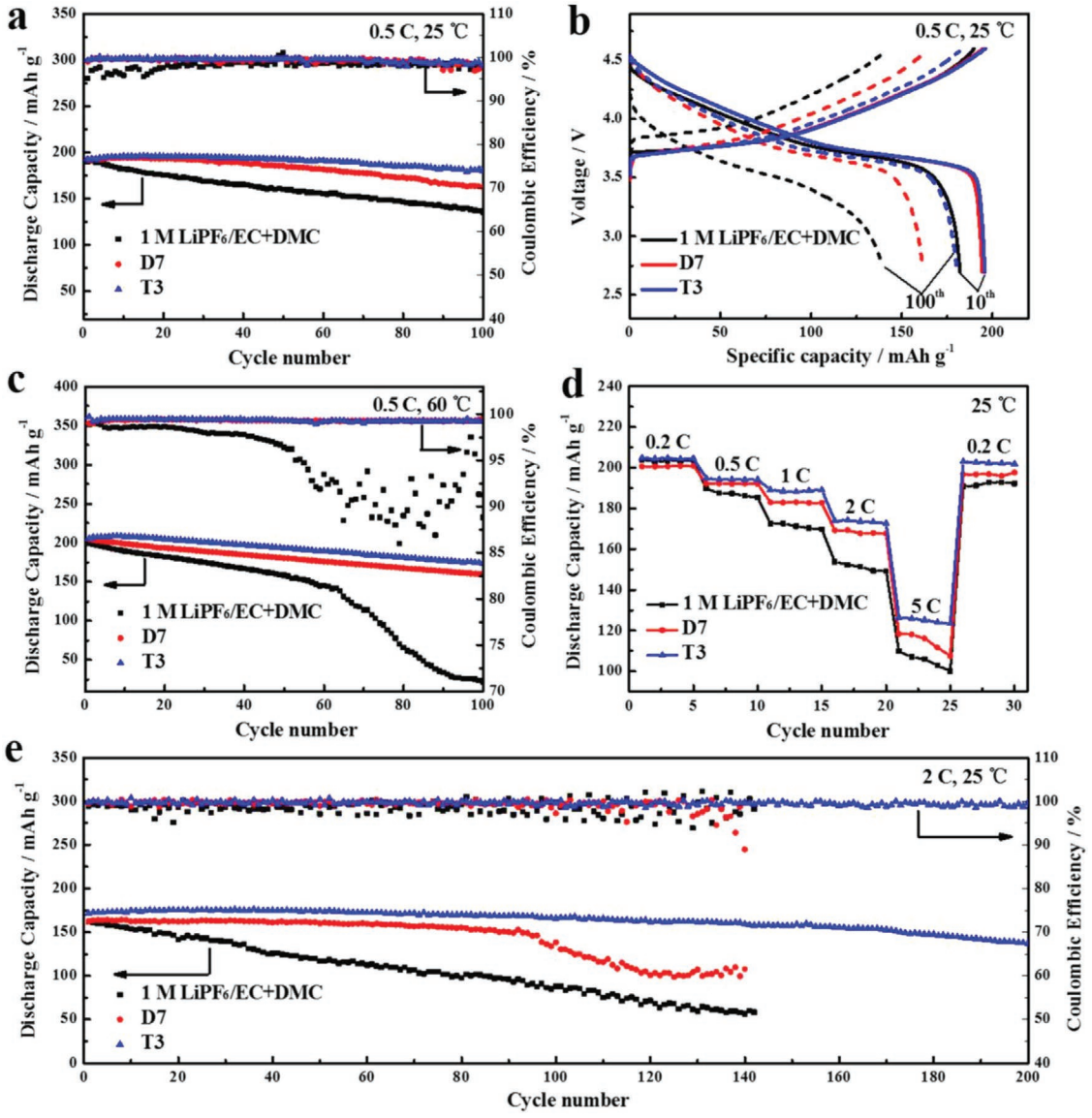

Figure 5. a) Cycling performance and b) charge/discharge voltage profiles of Li||NMC622 cells with 1 M $LiPF_6$/EC+DMC, D7, and T3 electrolytes at 0.5 C and 25 °C. c) High-temperature cycling performance with different electrolytes at 0.5 C and 60 °C. d) Rate performance with different electrolytes at 25 °C. e) Cycling performance with different electrolytes at 2 C and 25 °C. The voltage range of charge and discharge is 2.7–4.6 V. All the cells were conducted for formation cycles at 0.2 C for one cycle followed by 0.5 C for one cycle.

Supporting Information). Li metal surface after 100 h cycling in the commercial electrolyte show a crack and loose morphology, while the morphology of Li metal cycled after 100 h in T3 electrolyte is more flat and dense, owning to the less Li dendrites deposition (Figure S7d,e, Supporting Information).

2.4. Electrochemical Performance of Li||NMC622 Cells

The compatibility of the countersolvent electrolyte to the high-energy $LiNi_{0.6}Mn_{0.2}Co_{0.2}$ cathode was also evaluated using Li||NMC622 cells. The wide electrochemical windows of D7 and T3 electrolytes tested by using linear sweep voltammetry (LSV) are up to 5.5 V, which allows the NMC622 cathode to be charged to a high cut-off voltage of 4.6 V (Figure S8, Supporting Information). Meanwhile, aluminium current collector is passivated in T3 electrolyte at 4.6 V (Figure S9, Supporting Information). **Figure 5**a shows that the NMC622 cathode in T3 electrolyte significantly outperforms that in D7 and the $LiPF_6$-based electrolytes at 0.5 C and 25 °C with the charge/discharge voltage range of 2.7–4.6 V. In detail, the cell in T3 electrolyte enables a capacity retention of 93.5% after 100 cycles, which is much better than that in D7 (84.3%) and the $LiPF_6$-basd electrolyte (71.3%). The average CEs of NMC622 cathodes are 99.4%, 99.2%, and 98.1% for T3, D7, and the $LiPF_6$-based electrolytes, respectively. The charge/discharge voltage profiles of the 10th and 100th cycles in the different electrolytes at 0.5 C and 25 °C can be seen in Figure 5b. The charge/discharge voltage profiles

of the first formation cycles at 0.2 C and the second cycles at 0.5 C are provided in Figure S10 in the Supporting Information. Since the countersolvent TTE has a high boiling point (92 °C), the T3 countersolvent electrolyte also supports a good high-temperature tolerance. As can be seen from Figure 5c, the capacity of NMC622 cathode in the $LiPF_6$-based electrolyte deteriorates rapidly during the 100 cycles at 60 °C, leaving only 10.7% of its initial capacity with an average CE of only 94.9%. In contrast, the capacity of NMC622 in T3 electrolyte still maintains 84.6% after 100 cycles with a CE of 99.3%, which is better than the capacity retention of 78.3% in D7 over 100 cycles. As shown in Figure 5d, NMC622 cathode in T3 electrolyte also displays a high rate performance with discharge capacities of 204 mAh g^{-1} at 0.2 C, 194 mAh g^{-1} at 0.5 C, 188 mAh g^{-1} at 1 C, 173 mAh g^{-1} at 2 C, and 125 mAh g^{-1} at 5 C. The excellent rate performance of NMC622 cathode in T3 electrolyte partially attributed to its higher Li^+ transfer number (Figure S11 and Table S4, Supporting Information). In addition, the superior wettability of T3 with the separator also contributes to its good rate performance, which was characterized by the contact angle tests between the electrolyte and the separator (**Figure 6**a–c). The improved wettability between the T3 and the separator may offer a lower resistance of Li^+ transference. Figure 5e shows the cycling performance of the NMC622||Li batteries in different electrolytes at a high rate of 2 C. Only the cell with T3 electrolyte can maintain a stable cycling over 200 cycles at 2 C with a capacity retention of 80.1% and an average CE of 99.6% (Figure 5e). These results indicate that the countersolvent electrolyte is effective to improve the electrochemical performance of NMC622 cathodes.

The whole XPS survey and the atomic concentration on the surface of cathode materials can be seen in Figure S12a,b in the Supporting Information. It is clear that the F/C ratio of the cathode electrolyte interphase (CEI) formed in T3 electrolyte is higher than that in D7 and the $LiPF_6$-based electrolyte. The F 1s spectra in Figure S12c–e in the Supporting Information show that the CEI formed in T3 electrolyte has a stronger LiF peak (684.8 eV) and S−F&C−F peak, compared to the CEI formed in D7. And only a small amount of LiF peak and POF&C−F peak are founded in 1 M $LiPF_6$/EC+DMC. The high F-containing CEI formed on the NMC622 cathodes in T3 is more stable at high voltage and is favorable for suppressing parasitic reactions between the cathode and the electrolyte, which can be attributed to a good cycling performance. Remarkably, T3 electrolyte also has a good safety, since it is non-flammable. In contrast, the commercial and D7 electrolytes are flammable, making them unsuitable for the application in future batteries (Figure 6d–f).

3. Conclusion

In summary, the countersolvent is used to reduce the solvation degree of Li^+ cations with solvent molecules and increase the binding strength of Li^+ cations with FSI^- anions. The altered Li^+ coordination structure of the countersolvent electrolyte favors to form an LiF-rich SEI layer on Li metal, which suppresses Li dendrites and exhibits a high Li plating/stripping CE of >99%. The symmetric Li||Li cell with the T3 countersolvent electrolyte achieves an extremely long-term cycle life of >1000 h at a current density of 1 mA cm^{-2} and a capacity of 1 mAh cm^{-2}. The use of countersolvent electrolyte made it possible to obtain stable cycling of Li||NMC622 batteries under a high cut-off voltage (4.6 V) at both the room temperature (25 °C) and high temperature (60 °C).

4. Experimental Section

Electrolytes Preparation: DMC (Sigma–Aldrich, 99.9%) and TTE (Sinochem Lantian Co., Ltd., 99.9%) were both dried with 4 Å molecular sieves before use. LiFSI (99.9%) was received from Suzhou Yacoo Science Co., Ltd. and was used as received. The electrolytes were prepared by mixing LiFSI with DMC and TTE in a glove box filled with argon.

Electrochemical Measurements: The cathodes were made up of $LiNi_{0.6}Mn_{0.2}Co_{0.2}O_2$ (NMC622) active material, super P, and polyvinylidene fluoride with a mass ratio of 9.0:0.5:0.5, and N-methyl-2-pyrrolidone was applied as the dispersant. The typical weight density of active materials for an electrode sheet is 8 mg cm^{-2} and the areal capacity loading is 1.5 mAh cm^{-2}. Celgard 3501 separator was used in this study. Lithium metal was carefully scraped to expose a fresh lithium surface. The Land test system (CT2001A, Wuhan, China) was used for the charge and discharge testings with the voltage range of 2.7–4.6 V. LSV and cyclic voltammetry (CV) were carried out at a scan rate of 5 mV s^{-1}. The EIS was tested in a frequency range from 10 MHz to 0.1 Hz with an AC signal amplitude of 5 mV. LSV, CV, and EIS data were collected on the CHI 660C electrochemical workstation (CH, Shanghai, China). Li^+ transference numbers were calculated by the formulas of $t_{Li^+} = R_{cell} / R_{DC}$ through testing the alternating-current (AC) impedance and direct-current (DC) impedance using symmetric Li||Li cells. AC impedance (R_{cell}) was obtained from EIS. And DC impedance (R_{DC}) was obtained by carrying out a 10 mV DC polarization to obtain a stable current I_{DC} ($R_{DC} = V_{DC} / I_{DC}$). All the electrochemical measurements were conducted at 25 °C.

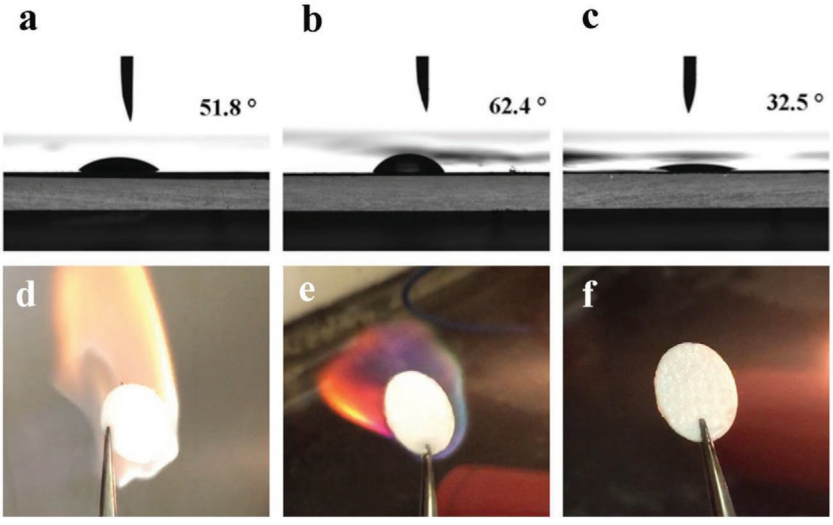

Figure 6. Contact angles between the electrolytes of a) 1 M $LiPF_6$/EC+DMC, b) D7, and c) T3 with celgard 3501 separators. Flammability tests of glass fibers saturated with d) 1 M $LiPF_6$/EC+DMC, e) D7, and f) T3 electrolytes.

Characterization: The morphology of lithium metal after 10 cycles of plating and stripping in Li||Cu cells was observed using SEM (HITACHI, SU8010, Japan). In order to study the composition of the SEI and CEI on the electrodes, the batteries were disassembled and the electrodes were washed with DMC in a glove box. The surface composition was tested by using XPS (PHI Quantro SXM ULVAC-PHI, Japan) with monochromatic Al Kα radiation at 280 kV, 55 eV. The Raman spectra were measured by using a Raman spectrometer (JY LabRam HR 800, Horiba Jobin Yvon, France). The wettability of the electrolyte with the separator was measured using a contact angle measurement (KRUSS K100 Laboratory Desktop, Krüss GmbH, Germany). NMR (PFG) experiments were performed on a 400 MHz NMR spectrometer on a double resonance probe head equipped with a *z*-gradient coil of maximum strength of 55 G cm^{-1}. ^{1}H, ^{19}F, and ^{7}Li diffusion coefficients were measured by using a standard stimulated echo pulse sequence, where the diffusion time (Δ) and the pulse length (δ) were set in the range of 100–1000 and 4–9 ms, respectively. The signal was accumulated over 16 transients with 2–5 s recycling delay by varying the gradient strength up to 16 increments. The diffusion coefficients were obtained by using Stejkal–Tanner equation plotting the intensity of NMR peaks against the gradient strength. All NMR measurements were performed at room temperature.

Computational Details: MD simulations were performed on the electrolytes using the Large-scale Atomic/Molecular Massively Parallel Simulator (http://lammps.sandia.gov.) package.[30] General Amber force fields parameters[31] and AM1-BCC charges[31,32] were used and generated by the ANTECHAMBER program in AmberTools for the solvent molecules.[33] The force field for Li and FSI were taken from previous publications.[34,35] The electrolyte systems were setup initially with the salt and solvent molecules distributed in the simulation boxes using Moltemplate (http://www.moltemplate.org/). The details of the calculated electrolytes are listed in Tables S2 and in the Supporting Information. To get the structure of the electrolyte, NPT runs were first performed at 330 K for 5 ns and then 298 K for 5 ns to ensure the equilibrium salt dissociation. Then, 10 ns long NVT runs were conducted and the last 5 ns were used to obtain the structure of electrolyte. Visualization of the structures is made by using VESTA and VMD software.[36,37] The electronic structure of LiFSI and TTE are calculated to compare their reduction stability using Gaussian 09 software package. The molecular orbital calculations are obtained through the B3LYP/6-311G** level with SMD implicit solvation model used (ε = 20) to describe the solvation effect.

Supporting Information

Supporting Information is available from the Wiley Online Library or from the author.

Acknowledgements

This work was funded by the Ministry of Science and Technology of China (nos 2019YFE010186 and 2018YFB0104400), and the National Natural Science Foundation of China (nos U1564205 and 51706117). The authors also thank Joint Work Plan for Research Projects under the Clean Vehicles Consortium at U.S. and China-Clean Energy Research Center (CERC-CVC2.0, 2016–2020), and thank Tsinghua University-Zhangjiagang Joint Institute for Hydrogen Energy and Lithium Ion Battery Technology.

Conflict of Interest

The authors declare no conflict of interest.

Keywords

countersolvent electrolytes, lithium-metal batteries, SEI, solvation structure

Received: October 30, 2019
Revised: January 23, 2020
Published online:

[1] D. Lin, Y. Liu, Y. Cui, *Nat. Nanotechnol.* **2017**, *12*, 194.
[2] J. Liu, Z. Bao, Y. Cui, E. J. Dufek, J. B. Goodenough, P. Khalifah, Q. Li, B. Y. Liaw, P. Liu, A. Manthiram, *Nat. Energy* **2019**, *4*, 180.
[3] X. Liang, Q. Pang, I. R. Kochetkov, M. S. Sempere, H. Huang, X. Sun, L. F. Nazar, *Nat. Energy* **2017**, *2*, 17119.
[4] C. Niu, H. Lee, S. Chen, Q. Li, J. Du, W. Xu, J.-G. Zhang, M. S. Whittingham, J. Xiao, J. Liu, *Nat. Energy* **2019**, *4*, 551.
[5] J. Qian, W. A. Henderson, W. Xu, P. Bhattacharya, M. Engelhard, O. Borodin, J.-G. Zhang, *Nat. Commun.* **2015**, *6*, 6362.
[6] D. Lin, Y. Liu, Z. Liang, H.-W. Lee, J. Sun, H. Wang, K. Yan, J. Xie, Y. Cui, *Nat. Nanotechnol.* **2016**, *11*, 626.
[7] Y. Liu, D. Lin, Z. Liang, J. Zhao, K. Yan, Y. Cui, *Nat. Commun.* **2016**, *7*, 10992.
[8] N. W. Li, Y. X. Yin, C. P. Yang, Y. G. Guo, *Adv. Mater.* **2016**, *28*, 1853.
[9] J. Zhao, L. Liao, F. Shi, T. Lei, G. Chen, A. Pei, J. Sun, K. Yan, G. Zhou, J. Xie, *J. Am. Chem. Soc.* **2017**, *139*, 11550.
[10] J. Zheng, M. H. Engelhard, D. Mei, S. Jiao, B. J. Polzin, J.-G. Zhang, W. Xu, *Nat. Energy* **2017**, *2*, 17012.
[11] X.-Q. Zhang, X. Chen, X.-B. Cheng, B.-Q. Li, X. Shen, C. Yan, J.-Q. Huang, Q. Zhang, *Angew. Chem., Int. Ed.* **2018**, *57*, 5301.
[12] F. Qiu, X. Li, H. Deng, D. Wang, X. Mu, P. He, H. Zhou, *Adv. Energy Mater.* **2019**, *9*, 1803372.
[13] M. Wang, L. Huai, G. Hu, S. Yang, F. Ren, S. Wang, Z. Zhang, Z. Chen, Z. Peng, C. Shen, D. Wang, *J. Phys. Chem. C* **2018**, *122*, 9825.
[14] X.-Q. Zhang, X. Chen, L.-P. Hou, B.-Q. Li, X.-B. Cheng, J.-Q. Huang, Q. Zhang, *ACS Energy Lett.* **2019**, *4*, 411.
[15] J. Wang, Y. Yamada, K. Sodeyama, C. H. Chiang, Y. Tateyama, A. Yamada, *Nat. Commun.* **2016**, *7*, 12032.
[16] L. Suo, Y.-S. Hu, H. Li, M. Armand, L. Chen, *Nat. Commun.* **2013**, *4*, 1481.
[17] X. Fan, L. Chen, X. Ji, T. Deng, S. Hou, J. Chen, J. Zheng, F. Wang, J. Jiang, K. Xu, C. Wang, *Chem* **2018**, *4*, 174.
[18] Y. Yamada, J. Wang, S. Ko, E. Watanabe, A. Yamada, *Nat. Energy* **2019**, *4*, 427.
[19] S. Chen, J. Zheng, D. Mei, K. S. Han, M. H. Engelhard, W. Zhao, W. Xu, J. Liu, J. G. Zhang, *Adv. Mater.* **2018**, *30*, 1706102.
[20] L. Yu, S. Chen, H. Lee, L. Zhang, M. H. Engelhard, Q. Li, S. Jiao, J. Liu, W. Xu, J.-G. Zhang, *ACS Energy Lett.* **2018**, *3*, 2059.
[21] J. Zheng, G. Ji, X. Fan, J. Chen, Q. Li, H. Wang, Y. Yang, K. C. DeMella, S. R. Raghavan, C. Wang, *Adv. Energy Mater.* **2019**, *9*, 1803774.
[22] F. Huang, G. Ma, Z. Wen, J. Jin, S. Xu, J. Zhang, *J. Mater. Chem. A* **2018**, *6*, 1612.
[23] G. Ma, L. Wang, X. He, J. Zhang, H. Chen, W. Xu, Y. Ding, *ACS Appl. Mater. Interfaces* **2018**, *1*, 5446.
[24] T. Doi, Y. Shimizu, M. Hashinokuchi, M. Inaba, *J. Electrochem. Soc.* **2017**, *164*, A6412.
[25] X. Ren, S. Chen, H. Lee, D. Mei, M. H. Engelhard, S. D. Burton, W. Zhao, J. Zheng, Q. Li, M. S. Ding, *Chem* **2018**, *4*, 1877.
[26] J. E. Katon, M. D. Cohen, *Can. J. Chem.* **1975**, *53*, 1378.
[27] J. Zheng, J. A. Lochala, A. Kwok, Z. D. Deng, J. Xiao, *Adv. Sci.* **2017**, *4*, 1700032.

[28] Q. Zhang, J. Pan, P. Lu, Z. Liu, M. W. Verbrugge, B. W. Sheldon, Y.-T. Cheng, Y. Qi, X. Xiao, *Nano Lett.* **2016**, *16*, 2011.
[29] L. Chen, X. Fan, E. Hu, X. Ji, J. Chen, S. Hou, T. Deng, J. Li, D. Su, X. Yang, *Chem* **2019**, *5*, 896.
[30] S. Plimpton, *J. Comput. Phys.* **1995**, *117*, 1.
[31] A. Jakalian, D. B. Jack, C. I. Bayly, *J. Comput. Chem.* **2002**, *23*, 1623.
[32] A. Jakalian, B. L. Bush, D. B. Jack, C. I. Bayly, *J. Comput. Chem.* **2000**, *21*, 132.
[33] J. Wang, W. Wang, P. A. Kollman, D. A. Case, *J. Mol. Graph. Model.* **2006**, *25*, 247.
[34] K. Shimizu, D. Almantariotis, M. F. C. Gomes, A. I. A. Pádua, J. N. Canongia Lopes, *J. Phys. Chem. B* **2010**, *114*, 3592.
[35] F. Chen, M. Forsyth, *Phys. Chem. Chem. Phys.* **2016**, *18*, 19336.
[36] K. Momma, F. Izumi, *J. Appl. Crystallogr.* **2011**, *44*, 1272.
[37] W. Humphrey, A. Dalke, K. Schulten, *J. Mol. Graph.* **1996**, *14*, 33.